

## 3D Spheroid-Based Tumor Invasion Assay



### Author

Brad Larson  
Agilent Technologies, Inc.  
Winooski, VT, USA

Jan Seldin  
Greiner Bio-One  
North America, Inc.  
Monroe, NC, USA

### Abstract

Establishment of *in vitro* models that mimic tumor invasion as part of the metastatic process are a critical part of oncology research. The need to incorporate multiple cell types, long-term kinetic analysis, methods to allow 3D invasion into the surrounding matrix, and appropriate detection and analysis, has made it difficult to create new models. The procedure described in this application note meets these needs through inclusion of advanced imaging capabilities allowing for capture of multiple images throughout a range of z-heights, using brightfield and fluorescence channels in a kinetic fashion. Final processed images, following stitching and z-projection, enable accurate cellular analysis to discern the invasive capabilities of 3D cellular structures over time.

## Introduction

Oncology drug discovery has been met with multiple challenges over the years. As cancers develop multiple mutations during carcinogenesis, targeted approaches to individual gene mutations common to many drug discovery campaigns have mostly limited efficacy. Conversely, the advancement of novel methods that focus on the inhibition of the invasive phenotype of metastasis offers greater potential for meaningful intervention, particularly due to the fact that most cancer patients die only after metastasis has occurred. For this approach to work, *in vitro* cell models used in early drug discovery should mimic as close as possible the complex metastatic process. Tumors *in vivo* exist as a three-dimensional (3D) mass of multiple cell types, including cancer and stromal cells. Therefore, incorporating a 3D spheroid-type cellular structure that includes co-cultured cell types forming a tumoroid provides a more predictive model than the use of individual cancer cells seeded in microplates. A further constraint is the need for long-term kinetic experiments to capture the invasion process which typically require multiple days. Thus, environment control of the assay is needed such that the cell viability of the spheroid is maintained over this long period and putative drug effects properly assessed. Finally, the only suitable readout for monitoring tumor invasion is microscopy due to the small size of the spheroid. To be effective in drug discovery, the microscope must have automated image capture, processing, and analysis to be able to cope with the multiple assay conditions, compounds tested, and kinetic images taken. This work will demonstrate a procedure for the generation of 3D spheroidal tumoroid structures, creation of a suitable invasion matrix, automated kinetic image-based monitoring, and cellular analysis of captured z-stacked images of tumor invasion.

U-87 and LN-229 glioblastoma multiforme (GBM) cell lines were used in this study as they have demonstrated phenotypic differences and metastatic ability.<sup>1</sup> Notably, the growth suppressing PTEN gene is mutated in U-87 cells, yet functions normally in LN-229 cells. Additionally, the human cytomegalovirus phosphotransferase protein UL-97 inhibits DNA elongation and replication and is absent from U-87 cells, but present in LN-229 cells.<sup>2</sup> This supports a more aggressive growth and invasion pattern for U-87 cells. Both cell types were co-cultured with fibroblasts to create 3D tumoroids more closely representing *in vivo* tumor conditions and allowed to invade through a protein matrix.

17-allylamino-17-demethoxygeldanamycin (17-AAG), known to inhibit the function of heat shock protein 90 (Hsp90), a chaperone protein that stabilizes proteins required for tumor growth, was used here to inhibit potential tumor invasion.<sup>3</sup> Quantification of kinetic captured images was used to characterize the invading potential of inhibited and uninhibited tumoroid cultures.

## Materials and methods

### Materials

#### Cells

U-87 GBM cells expressing GFP were generously donated by Dr. Sachin Katyal (University of Manitoba, Winnipeg, Manitoba, Canada). LN-229 GBM cells (part number CRL-2611) were obtained from ATCC (Manassas, VA). Human neonatal dermal fibroblasts expressing RFP (part number cAP-0008RFP) were purchased from Angio-Proteomie (Boston, MA).

#### Experimental components

Matrigel basement membrane matrix, phenol red-free (part number 356237) was purchased from Corning Life Sciences (Corning, NY). The selective Hsp90 inhibitor 17-AAG (part number 1515) was sourced from Tocris Bioscience (Avonmouth, Bristol, UK). CellTracker Deep Red dye (part number C34565) was purchased from Thermo Fisher Scientific (Waltham, MA). 96-well, cell-repellent, polystyrene, round bottom, clear, sterile, microplates with lid (part number 650979) were generously donated by Greiner Bio-One North America, Inc. (Monroe, NC).

#### Agilent BioTek Cytation 5 cell imaging multimode reader

Cytation 5 is a modular multimode microplate reader combined with an automated digital microscope. Filter- and monochromator-based microplate reading are available, and the microscopy module provides up to 60x magnification in fluorescence, brightfield, color brightfield, and phase contrast. The instrument can perform fluorescence imaging in up to four channels in a single step. With special emphasis on live cell assays, Cytation 5 features shaking, temperature control to 65 °C, CO<sub>2</sub>/O<sub>2</sub> gas control and dual injectors for kinetic assays and is controlled by integrated Agilent BioTek Gen5 microplate reader and imager software, which also automates image capture, analysis, and processing. The instrument was used to kinetically monitor 3D tumoroid activity over the incubation period.

### Agilent BioTek BioSpa 8 automated incubator

The BioSpa 8 automated incubator links Agilent BioTek readers or imagers together with Agilent BioTek washers and dispensers for full workflow automation of up to eight microplates. Temperature, CO<sub>2</sub>/O<sub>2</sub> and humidity levels are controlled and monitored through the Agilent BioTek BioSpa software to maintain an ideal environment for cell cultures during all experimental stages. Test plates were incubated in the BioSpa to maintain proper atmospheric conditions for a period of seven days and automatically transferred to the Cytation 5 every twelve hours for brightfield and fluorescence imaging.

### Agilent BioTek MultiFlo FX multimode dispenser

The MultiFlo FX is a modular, upgradable reagent dispenser that can have as many as two peri-pump (8 tube dispensers), two syringe pump dispensers, and a strip washer. The syringe and washer manifolds can be configured for plate densities from 6- to 384-well.

## Methods

### Cell preparation and tumoroid formation

Prepared U-87 and fibroblast cells were each harvested and combined in a final concentration of  $2.5 \times 10^4$  cells/mL for each cell type in complete medium. After dispensing 100  $\mu$ L of cell suspension into appropriate microplate wells, the microplate was incubated at 37 °C/5% CO<sub>2</sub> for 48 hours to allow cells to aggregate into tumoroids. This process was repeated using LN-229 cells stained with CellTracker Deep Red dye and fibroblast cells at the same concentrations and volumes.

### Invasion matrix preparation

Upon completion of tumoroid formation, 70  $\mu$ L of complete medium was robotically removed from each well, and the tumoroid plate placed on ice in a refrigerator for five minutes to cool the cells. Matrigel matrix was then thawed on ice. 17-AAG was diluted to a 2x concentration of 20,000 nM in invasion media and used to create an eight-point titration from 20,000 nM to 0 nM using serial 1:4 dilutions. The inhibitor titrations were further diluted to a 1x concentration by combining with either invasion media or Matrigel matrix. With the plate still on ice, 70  $\mu$ L of Matrigel matrix plus titrated compound were added to each well containing tumoroids, then overlaid with 100  $\mu$ L invasion media containing titrated compound. The microplate was centrifuged at 300  $\times$  g for five minutes in a swinging bucket centrifuge that was previously set to 4 °C for tumoroid positioning, then transferred to a 37 °C/5% CO<sub>2</sub> incubator for one hour to initiate gel formation.

### Tumor invasion assay performance

After gel formation was complete, the microplate was transferred to BioSpa 8, where the software was programmed such that the microplate was automatically transferred to Cytation 5 for brightfield and fluorescent imaging of the wells every twelve hours over the seven-day incubation period. Table 1 lists the settings used to perform automated image capture of each sample well.

**Table 1.** Automated 3D tumoroid invasion imaging parameters.

Imaging Parameters	
Brightfield Imaging Channel	Complete 3D invading structure
GFP Imaging Channel	U-87 Cells expressing GFP
RFP Imaging Channel	Fibroblasts expressing RFP
CY5 Imaging Channel	LN-229 Cells stained with CellTracker Deep Red dye
Objective	4x
Montage	3 Rows by 2 columns
Montage Overlap	Auto for stitching
Z-Stack	20 Slices
Z-Stack Step Size	53.8 $\mu$ m (Default for 4x objective)

### Image processing

Individual image tiles from each z-plane captured using the three by two montage were then stitched together (Table 2).

**Table 2.** Image stitching parameters.

Imaging Stitching Parameters	
Registration Channel	Brightfield
Fusion Method	Linear blend
Crop Stitched Image to Remove Black Rectangles on the Borders	Checked
Downsize Final Image	Checked (52.62%)

A single image projection was then created from the 20-slice stitched z-stack (Table 3). The focus stacking method was chosen, which automatically selects the most in focus pixel from each image in the stack for inclusion in the final projection. This allows the most accurate analysis to be carried out on each invading tumoroid at each time point.

**Table 3.** Image z-projection parameters.

Imaging Z-Projection Parameters	
Channel 1	Stitched[Brightfield]
Method	Focus stacking
Size of Maximum Filter	11 px
Z-Slices Included	1 to 20
Channels 2 to 4	Stitched[GFP], Stitched[RFP], Stitched[CY5]
Method (Channels 2 to 4)	Use settings of channel 1

## Tumoroid invasion analysis

Primary mask cellular analysis criteria (Table 4) were applied using the brightfield channel to automatically place object masks around the entire invading structure in each final image. Secondary mask cellular analysis criteria (Table 5) were also applied to place an additional mask around noninvasive cells remaining within the original spherical tumoroid structure.

**Table 4.** Primary mask analysis parameters.

Primary Cellular Analysis Parameters	
Channel	ZProj[Stitched[Brightfield]]
Threshold	25,000
Background	Light
Split Touching Objects	Unchecked
Fill Holes in Masks	Checked
Minimum Object Size	300 $\mu\text{m}$
Maximum Object Size	2,000 $\mu\text{m}$
Include Primary Edge Objects	Checked
Analyze Entire Image	Checked
Advanced Detection Options	
Rolling Ball Diameter	2,000
Image Smoothing Strength	0
Evaluate Background On	5% of lowest pixels
Analysis Metric	
Metric of Interest	Object area

**Table 5.** Secondary mask analysis parameters.

Secondary Cellular Analysis Parameters	
Channel	ZProj[Stitched[Brightfield]]
Measure Within a Secondary Mask	Include primary mask
Reduce Primary Mask	1 $\mu\text{m}$
Threshold	12,000
Smooth	7
Fill Holes in the Mask	Unchecked
Analysis Metric	
Metric of Interest	Object Area_2[ZProj[Stitched[Brightfield]]]

## Results and discussion

### Raw image processing prior to cellular analysis

During the seven-day incubation period, uninhibited U-87/fibroblast tumoroids continued to increase in size, as well as invade into the protein matrix. To ensure that the entire invading structure, including invadopodia, was captured in the X- and Y-axes, regardless of size, multiple images were taken on a single z-plane in a montage format (Table 1). Figure 1 illustrates four of the six images that were captured containing portions of the invading structure.

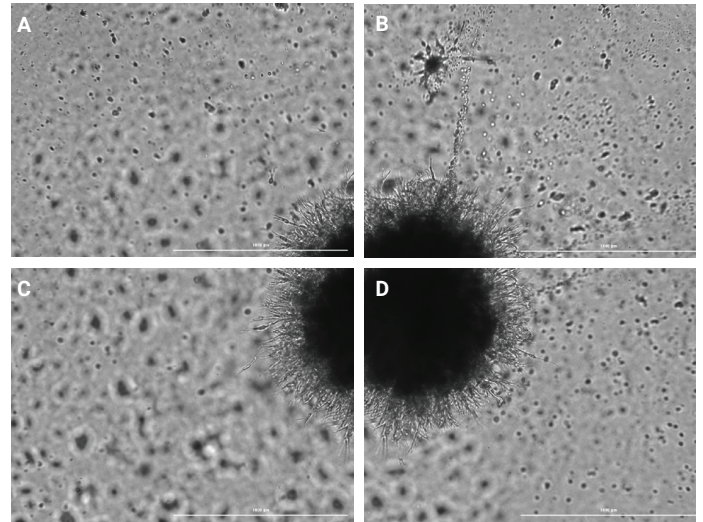


**Figure 1.** U-87/fibroblast 4x brightfield imaging showing (A to D) four image tiles containing the invading tumoroid of interest.

As invasion proceeds, proteins and cells invade on multiple planes within the Z-axis. Therefore, images were automatically taken across a range of z-heights so that all portions of the overall structure were in focus in the final z-projected images (Figures 2A to 2D).

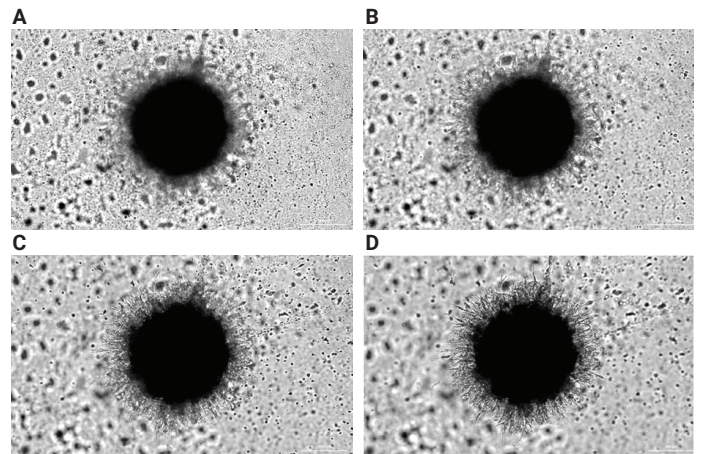


**Figure 2.** U-87/fibroblast 4x brightfield imaging showing (A to D) four of the twenty images captured at multiple z-planes as part of the z-stack and combined into the final z-projection.



### Imaging of U-87/fibroblast individual co-cultured cell types

In addition to brightfield imaging, montage tiles and z-stacked layers were also captured using the GFP and RFP channels. Overlaying images tracks invasion of the entire structure (Figure 3).

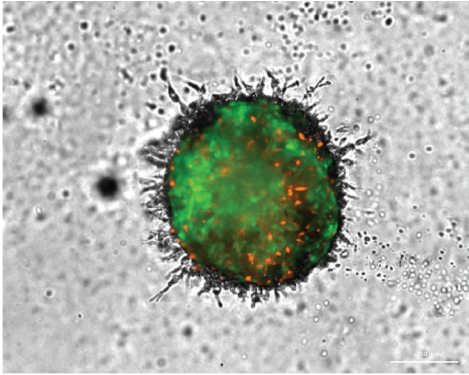


**Figure 3.** Brightfield and fluorescent overlaid z-projected image of U-87/fibroblast co-cultured cell model.

By viewing the fluorescent signal emitted by each co-cultured cell type, in comparison to the brightfield signal from the entire structure, individual cell migration can be observed. In the case of the U-87/fibroblast model, the brightfield image demonstrates extensive invadopodia extending out from the original propagating tumoroid (Figure 4A). From the GFP image in Figure 4B, it is evident that GFP-expressing U-87 cells follow invadopodia invasion into the matrix. This contrasts to the RFP image in Figure 4C confirming that RFP-expressing fibroblasts exhibit little to no migratory ability within this experimental model.

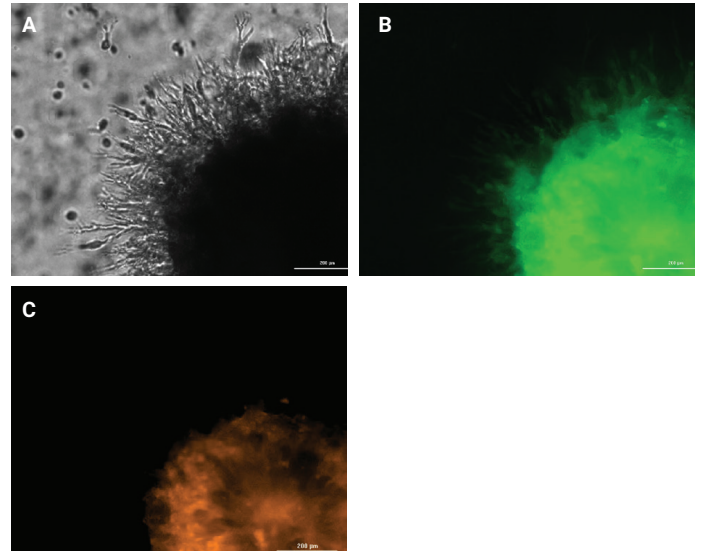


**Figure 4.** Confirmation of invasion by individual cell types. (A) Total tumoroid invasion via overlaid GFP, RFP, and brightfield channels. Individual cellular invasion by (B) GFP-expressing U-87 cells, or (C) RFP-expressing fibroblast cells. Digitally zoomed 4x images, 2 × 3 montage, 20-plane z-stack.

### Kinetic image capture

Finally, z-projected images are captured kinetically every 12 hours to observe phenotypic changes in the U-87/fibroblast co-cultured tumoroids following treatment with varying concentrations of 17-AAG. Uninhibited tumoroids, as expected, demonstrate a highly invasive nature<sup>4</sup>, exhibiting an increase in the size of the tumoroid body as well as a dramatic increase in invadopodia (Figure 5).

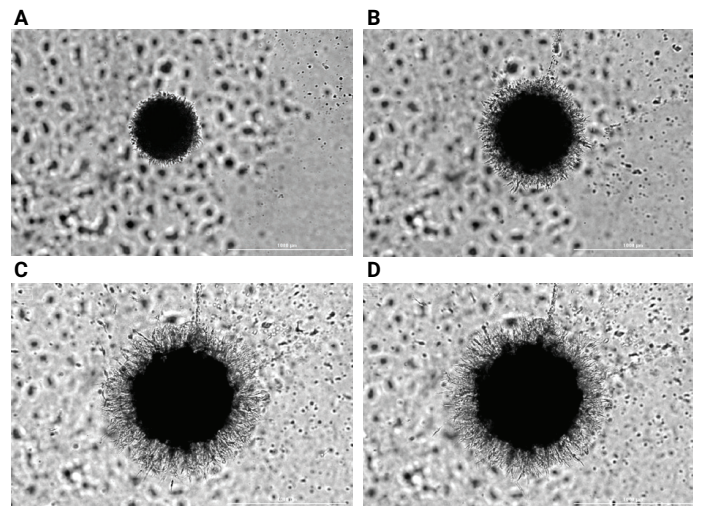


**Figure 5.** U-87/fibroblast tumoroid invasive potential over time, 4x brightfield images, 2 × 3 montage, 20-plane z-stack. (A) 0 hours; (B) 48 hours; (C) 120 hours; (D) 168 hours.

### LN-229/Fibroblast tumoroid analysis

LN-229/fibroblast tumoroid imaging was also conducted in the same manner as that for the U-87/fibroblast tumoroids. This was done to compare differences in growth and invadopodia production between GBM cell types known to be highly invasive (U-87) and those with less invasive ability (LN-229).<sup>5</sup> Changes in the complete 3D structure were observed using the overlaid brightfield and fluorescent images (Figure 6A), while individual LN-229 or fibroblast invasion was monitored by signal captured with the individual CY5 or RFP channels, respectively (Figures 6B and 6C).

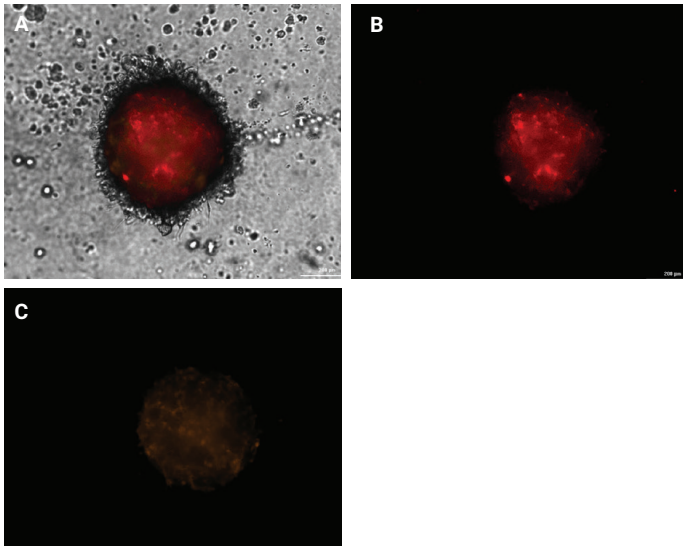


**Figure 6.** Imaging of LN-229/fibroblast co-cultured cell model. (A) Total tumoroid invasion via overlaid CY5, RFP, and brightfield channels. Individual cellular invasion by (B) CellTracker Deep Red stained LN-229 cells; or (C) RFP-expressing fibroblast cells. Digitally zoomed 4x images, 2 × 3 montage, 20-plane z-stack.

When comparing kinetic brightfield images from the two co-cultured cell types, it is evident that LN-229/fibroblast tumoroids propagate over time, as seen by the increase in spheroid size (Figure 7), but do not exhibit the invasive properties clearly demonstrated by U-87/fibroblast tumoroids over the same incubation period (Figure 5).

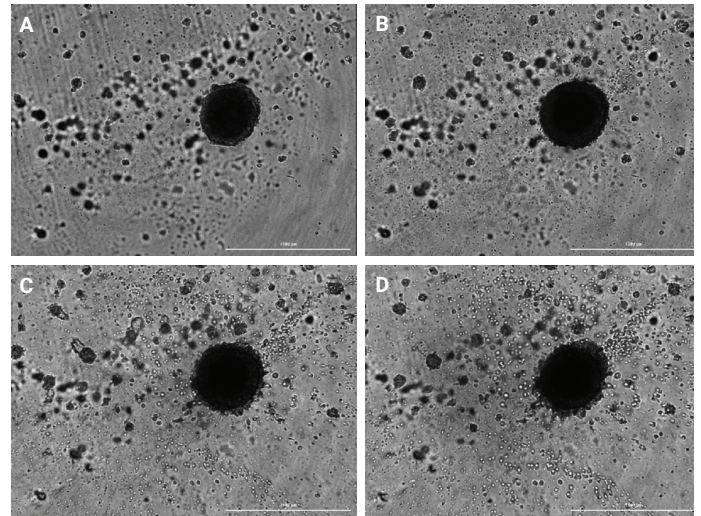


**Figure 7.** LN-229/fibroblast tumoroid invasive potential over time, 4x brightfield images, 2 × 3 montage, 20-plane z-stack. (A) 0 hours; (B) 48 hours; (C) 120 hours; (D) 168 hours.

### Agilent BioTek Gen5 Image+ based cellular analysis of tumoroid invasion

In addition to qualitative assessments of tumoroid phenotypic changes, quantification of the extent of invasion was also carried out using the stitched, z-projected brightfield images. Two separate cellular analyses were performed following treatment with the 17-AAG titration. In the first, the primary cellular analysis capabilities available in Gen5 Image+, and the criteria listed in Table 4 used changes in brightfield signal within the image between cellular containing pixels and background to place detailed object masks around the complete invading 3D structure, despite the level of compound treatment (Figure 8).

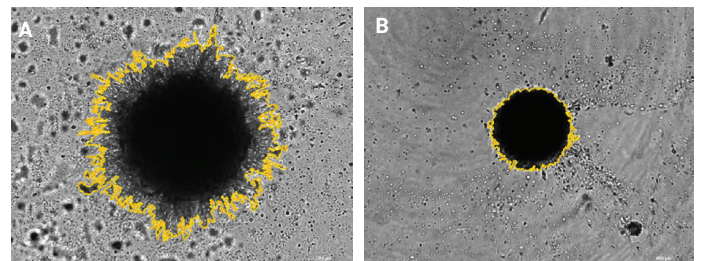


**Figure 8.** Invading tumoroid object masking. Zoomed 4x brightfield images of U-87/fibroblast tumoroids, 2 × 3 montage, 20-plane z-stack. (A) 0 μM 17-AAG treatment and (B) 10 μM 17-AAG treatment. Primary masks around cells and invadopodia.



The area covered by the entire tumoroid for each captured image over time was then calculated. Values from subsequent time points were then divided by the area value calculated at time 0 for the specific tumoroid to normalize results and account for variability in tumoroid size following cell dispensing and aggregation. Area ratios were then plotted (Y-axis) with regards to time (X-axis) (Figure 9).

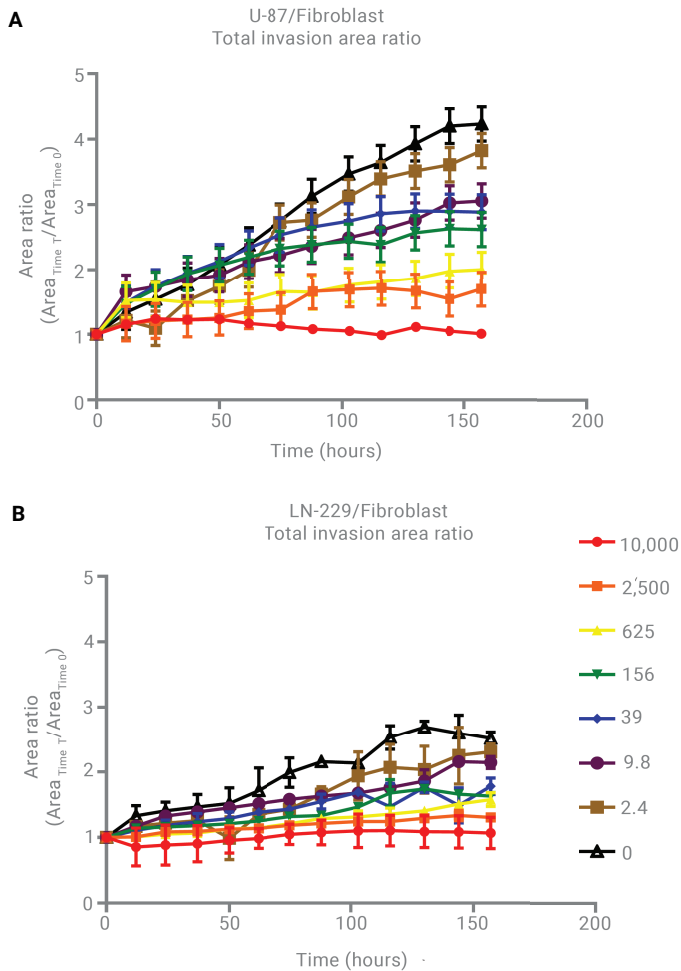


**Figure 9.** Kinetic total tumoroid area ratios. Area ratios plotted for (A) U-87/fibroblast tumoroids, or (B) LN-229/fibroblast tumoroids following 0 to 7-day treatments with 17-AAG concentrations ranging from 10,000 to 0 nM. Area ratio calculated by the following formula:  $(Area_{Time T} / Area_{Time 0})$ .

From the results seen in Figure 9, it is apparent that both U-87/fibroblast and LN-229/fibroblast tumoroids propagate within the Matrigel matrix when unimpeded over the seven-day incubation period. It can also be seen that the compound 17-AAG is able to limit, or even completely stop, tumoroid growth in a dose-dependent manner, as expected.<sup>3</sup> What is also clear from the total area ratio graphs is the increased rate of growth for the complete 3D structure exhibited by U-87/fibroblast tumoroids compared to those where LN-229 cells are co-cultured with fibroblasts. Increases in the area covered by the entire tumoroid are approximately 2x over time for tumoroids cultured with U-87 cells (ratio: 4.4) compared to those cultured with LN-229 cells (ratio: 2.4).

### Agilent BioTek Gen5 Image Prime-based cellular analysis of tumoroid invasion

A second cellular analysis was also performed using the primary and secondary cellular analysis capabilities available in Gen5 Image Prime, and the criteria listed in Table 5, to measure the area solely covered by noninvading cells within the tumoroid. To determine the metastatic ability of 3D *in vitro* models, both uninhibited, or following treatment, it is important to distinguish between area covered by cells within the original tumoroid and that covered by invadopodia. As the more densely packed noninvasive, propagating cells appear darker compared to invadopodia in a brightfield image (Figure 10A), this additional change in signal within the original mask allows placement of a secondary mask to exclude the invading areas of each tumoroid and separate the area covered by the two portions of the entire 3D structure (Figure 10).

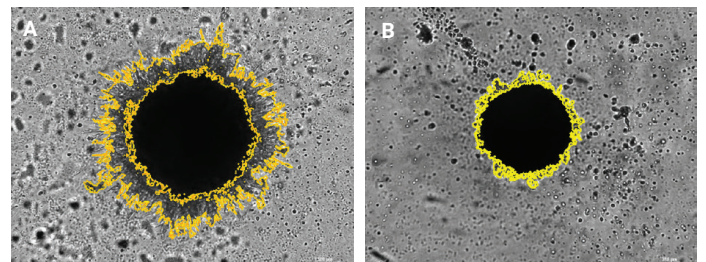


**Figure 10.** Invading and main tumoroid area object masking. Zoomed 4x brightfield 2 x 3 montage, 20-plane z-stack images of (A) uninhibited U-87/fibroblast tumoroids; or (B) uninhibited LN-229/fibroblast tumoroids. Exterior primary masks around cells and invadopodia, and interior secondary masks around noninvading cellular structure only.

By applying the secondary mask around noninvading portions of the tumoroid, differences in the invasive qualities of the two GBM cell types then becomes clear.

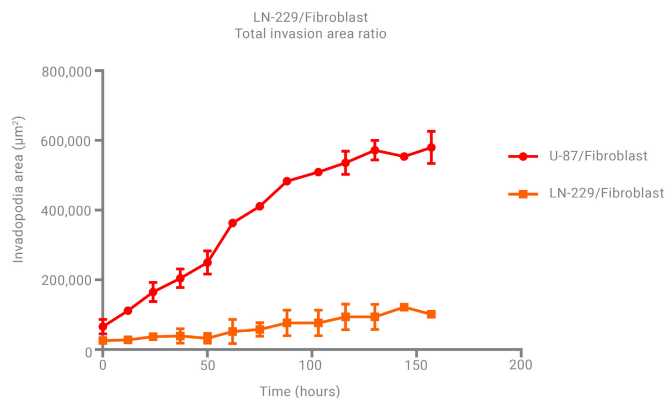


**Figure 11.** Kinetic uninhibited U-87 and LN-229 co-cultured tumoroid kinetic invadopodia areas. Calculated invadopodia area over time for nontreated U-87/fibroblast and LN-229/fibroblast tumoroids. Invadopodia area calculated by the following formula:  $(\text{Total Area}_{\text{time T}} - \text{Noninvading Area}_{\text{time T}})$ .

The area covered by invadopodia for U-87/fibroblast tumoroids increases dramatically over the seven day incubation period. LN-229/fibroblast tumoroids, by comparison, show little increase in invadopodia over the same time (Figure 11). This dual analysis, therefore, has the potential to determine not only how rapidly tumoroid cells are propagating, but also the invasive nature of the cell model.

## Conclusion

Application of advanced cellular imaging capabilities, such as taking multiple images on a single z-plane as well as in a z-stack, allows all portions of an invading 3D cellular tumoroid structure to be captured in focus. When stitched and projected to a final image, accurate analysis can then be performed. The ability to view entire tumoroids via brightfield imaging, as well as individual cell types through fluorescent imaging, also allows for determination of the invasive properties of each co-cultured cell type within the included cell model. Inclusion of label-free cellular analysis, carried out on brightfield images, can then quantify not only propagative qualities, but also the specific invasive nature of *in vitro* 3D cell models when uninhibited and in response to test molecules.

## References

1. Furnari, F. B. *et al.* Growth Suppression of Glioma Cells by PTEN Requires a Functional Phosphatase Catalytic Domain. *Proc. Natl. Acad. Sci. USA* **1997**, *94*(23), 12479–84.
2. McFall, T. B. Identification of HCMV UL97 in GBM Cell Lines and a Possible Role for Ganciclovir. Master's Dissertation, Northern Michigan University, Marquette, MI, **2014**.
3. Beckner, M. E. *et al.* Identification of ATP Citrate Lyase as a Positive Regulator of Glycolytic Function in Glioblastomas. *Int. J. Cancer*. **2010**, *126*(10), 2282–95.
4. Formolo, C. A. *et al.* Secretome Signature of Invasive Glioblastoma Multiforme. *J. Proteome Res.* **2011**, *10*(7), 3149–59.
5. Mallawaarachy, D. M. *et al.* Membrane Proteome Analysis of Glioblastoma Cell Invasion. *J. Neuropathol. Exp. Neurol.* **2015**, *74*(5), 425–41.

[www.agilent.com/lifesciences/biotek](http://www.agilent.com/lifesciences/biotek)

For Research Use Only. Not for use in diagnostic procedures.

RA44412.5340972222

This information is subject to change without notice.

© Agilent Technologies, Inc. 2018, 2022  
Printed in the USA, April 8, 2022  
5994-3393EN